Bioprocess and Biosystems Engineering (2023) 46:1569–1578
https://doi.org/10.1007/s00449-023-02920-2

RESEARCH PAPER

Green synthesis of zinc and nickel dual-doped cerium oxide nanoparticles: antioxidant activity and cytotoxicity effects

Pegah Mahmoodi[1] · Alireza Motavalizadehkakhky[2,3] · Majid Darroudi[4] · Jamshid Mehrzad[1,3] · Rahele Zhiani[3,5]

Received: 30 June 2023 / Accepted: 7 August 2023 / Published online: 12 September 2023

Abstract

Cerium oxide nanoparticles (CeO_2-NPs) and Zn–Ni dual-doped CeO_2-NPs were synthesized through a green approach by the implication of *zucchini peel* (*Cucurbita pepo*) extract as a capping and reduction agent. All the synthesized samples were studied by the results of FTIR, UV–Vis, XRD, and FESEM/EDAX/PSA analyses. The Zn–Ni dual-doped CeO_2-NPs contained a spherical morphology and their size was observed to increase at higher temperatures. The conducted MTT assay on the Huh-7 cell line displayed 50% of cells annihilation as a result of using undoped CeO_2-NPs and Zn–Ni dual-doped CeO_2-NPs at the inhibitory concentrations (IC_{50}) of 700 and 185.4 µg/mL, respectively. We also evaluated the enzymatic functionality of *SOD* and *CAT* of undoped CeO_2-NPs and dual-doped NPs and found it to be dose dependent. Moreover, Zn–Ni dual-doped CeO_2-NPs intensified the *CAT* activity without causing any changes in *SOD* activity in similar concentrations.

✉ Alireza Motavalizadehkakhky
Amotavalizadeh@iau-neyshabur.ac.ir

✉ Majid Darroudi
majiddarroudi@gmail.com; darroudim@mums.ac.ir

1 Department of Biochemistry, Neyshabur Branch, Islamic Azad University, Neyshabur, Iran

2 Department of Chemistry, Neyshabur Branch, Islamic Azad University, Neyshabur, Iran

3 Advanced Research Center for Chemistry, Biochemistry and Nanomaterial, Neyshabur Branch, Islamic Azad University, Neyshabur, Iran

4 Department of Basic Medical Sciences, Neyshabur University of Medical Sciences, Neyshabur, Iran

5 New Materials Technology and Processing Research Center, Department of Chemistry, Neyshabur Branch, Islamic Azad University, Neyshabur, Iran

Graphical Abstract

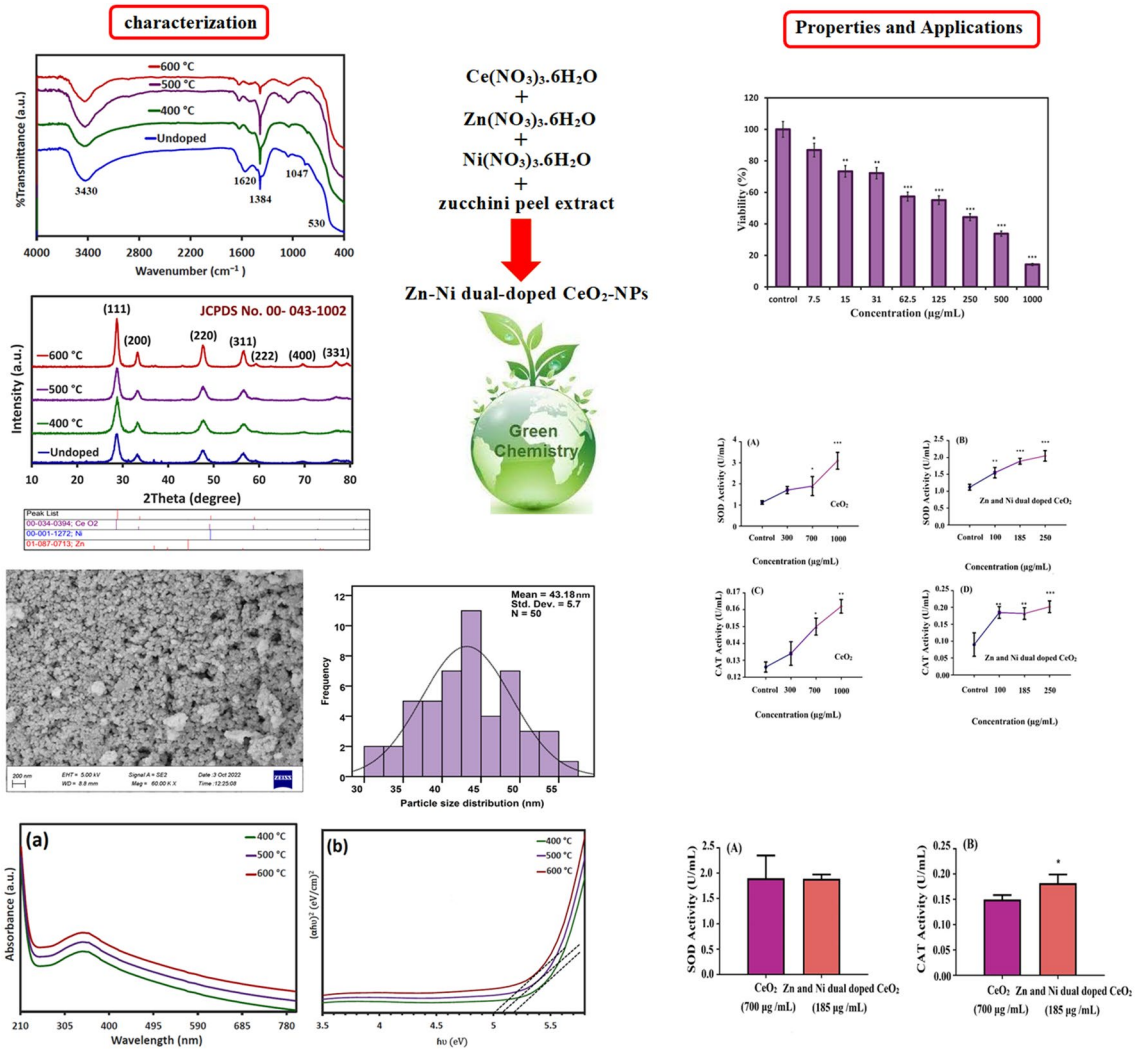

Keywords Green synthesis · Zinc and nickel dual-doped cerium oxide nanoparticles · Antioxidant activity · Cytotoxicity

Abbreviations

DMEM	Dulbecco's modified Eagle's medium
DMSO	Dimethyl sulfoxide
PBS	Phosphate-buffered saline
FBS	Fetal bovine serum
MB	Methylene blue
IC_{50}	Half-maximal inhibitory concentration
MTT	3-(4,5-Dimethylthiazol-2-yl)-2,5-diphenyl-2H-tetrazolium bromide
DTA	Thermogravimetric analysis (TGA) and differential thermal analysis
FT-IR	Fourier-transform infrared
XRD	X-ray powder diffraction
PSA	Particle size analysis
FESEM	Field emission scanning electron microscopy
EDX	Energy-dispersive X-ray
DRS	Diffuse reflectance spectroscopy
SOD	Superoxide dismutase
CAT	Catalase

Introduction

Also known as nanoceria, CeO_2-NPs have a fluorite crystalline structure along with a high surface area and the capacity for oxygen vacancy that has turned this substance into a distinctive catalyst [1]. The characteristics of its oxygen vacancies are distinguished by the existing Ce (III) atoms at the center with surrounding adjacent Ce (IV) atoms [2]. The interest of many scientists in the fields of biological

sciences, chemistry, engineering, etc. is invested in nanoceria [3]. Among its various biological applications, nanoceria has achieved very good results in the field of diseases caused by free radicals such as autoimmune cases similar to cancer, multiple sclerosis, and Alzheimer's [4], while it also proved to contain potent anti-inflammatory properties due to auto-regenerative free radical scavengers [5]. Human cells prevalently produce reactive oxygen species (ROSs) as unavoidable by-products through various metabolic processes that operate by oxidation–reduction reactions. The balance between the generation and neutralization of ROS can be altered in some physiological conditions, in which the amount of produced ROS exceeds the antioxidant capacity of the body for their removal and result in the induction of oxidative stress [6, 7]. This result can operate as the fundamental source of numerous pathophysiological disorders such as cancer, multiple sclerosis, stroke, amyotrophic lateral sclerosis (ALS), Parkinson, and Alzheimer's [8]. The most general ROSs involve H_2O_2, O_2^- and $OH^{\bullet}$, while *SOD* and *CAT* stand as the two most important antioxidant enzymes with defensive responsibilities against them [9]. Moreover, the removal of these unpaired electrons can be facilitated by the implication of an appropriate transition metal such as Ce^{3+}, similar to the process of *SOD* activity that causes the production of H_2O_2, which is removed by *CAT* activity in the next step [10]. The switch between Ce^{3+}/Ce^{4+} seems to be related to the redox enzyme mechanism. Metals serve as co-factors for catalyzing flexible redox reactions in tissues and cells. Previous reports have indicated the higher ratios of Ce^{3+}/Ce^{4+} as the most suitable scenario for the *SOD*-memic action of Ce, which is associated with the fact that Ce^{3+} is the only possible state with the option of oxidation to produce H_2O_2 [11, 12]. According to recent research on CeO_2-gadolinium (Gd), a high ratio of Ce^{3+}/Ce^{4+} can exhibit stronger *SOD* mimetic and anticancer activity [13], while another study revealed the ability of cerium oxide nanoparticles to induce *CAT* mimetic function. This function is correlated with the reduced level of Ce^{3+} state that is in opposition to the connection between surface charge and O^{-2} scavenging possessions. This procedure is preferred for the low Ce^{3+}/Ce^{4+} ratio conditions [14, 15]. Interestingly, one research demonstrated the ineffectiveness of pH changes, phosphate anions, and existing components in cell culture media on the *CAT* mimetic activity of Ce^{+4} nanoparticles [16]. The properties of scavenging oxygen and nitrogen radicals of CeO_2-NPs can cause synergistic effects in conjugation with *CAT* and *SOD* enzymes [17]. Hypoxia is a key factor in drug resistance, metastasis, and consequently cancer recurrence. In conformity with recent studies, CeO_2-NPs can catalyze H_2O_2 and produce oxygen with its *CAT* activity to subsequently exert its anticancer effect by improving hypoxia conditions [18]. Although antioxidants act as protectors at the pH of 7 in normal cells, their toxicity at the acidic pH of cancer cells has been observed as well. Considerably, the applicability of CeO_2-NPs as cytotoxic and protective agents in cancer treatment was approved, while the facilitation of high base levels of ROS in cancer cells by pro-oxidants resulted in their recognition as potential chemotherapeutic drugs [19, 20]. There are many limitations to the usage of conventional antioxidants such as their unavailability and weak penetration into the brain cells [21], which resulted in demands for proper antioxidants with the ability to overcome these problems and provide successful caring procedures for neurological disorders. Furthermore to the antioxidant properties of CeO_2-NPs that can neutralize inflammation and nerve damage factors, they can also progress into the blood–brain barrier and find their way to the central nervous system through the aid of their small sizes [4, 10]. The innovation of our work was the exertion of *zucchini peel* extract as a new reduction agent and stabilizer for controlling the particle size of Zn–Ni dual-doped CeO_2-NPs during the synthesizing process, while duel-doped Ni and Zn metals were applied to improve their antioxidant properties. We also included a discussion on the cytotoxicity and *SOD* and *CAT* activity of Zn–Ni dual-doped CeO_2-NPs in Huh-7 cell lines.

Method and materials

Materials

All materials used in this experiment had a high percentage of purity. The *zucchini* plant with the scientific name *Cucurbita pepo* was bought from a hypermarket in Mashhad, Iran. ($Ce(NO_3)_3{\cdot}6H_2O$), ($Zn(NO_3)_3{\cdot}6H_2O$), and ($Ni(NO_3)_3{\cdot}6H_2O$) salts were purchased from Sigma-Aldrich and Merck company. MTT, DMSO, trypsin, FBS, PBS, DMEM media, streptomycin, and penicillin (100 mg/mL) were bought from Sigma. *SOD* and *CAT* activity assay kits were obtained from TEB PAZHOUHAN RAZI (TPR) company.

Extraction of Zucchini peel

Initially, 50.0 g of clean *zucchini peel* was weighed and cut into small pieces to be mixed with 250.0 mL of deionized water and stirred at 50 °C for 3 h. Thereafter, Whatman 'filter paper was used to obtain the required extract, which was kept at 4 °C for the upcoming sections.

Synthesis of Zn–Ni dual-doped CeO_2-NPs

To synthesize Zn–Ni dual-doped CeO_2-NPs, we initially prepared the solutions of salts $Ce(NO_3)_3{\cdot}6H_2O$ (50.0 mL, 0.5 M) (A), $Zn(NO_3)_3{\cdot}6H_2O$ (20.0 mL, 5%) (B), and $Ni(NO_3)_3{\cdot}6H_2O$ (20.0 mL, 5%) (C). Next, the B and C

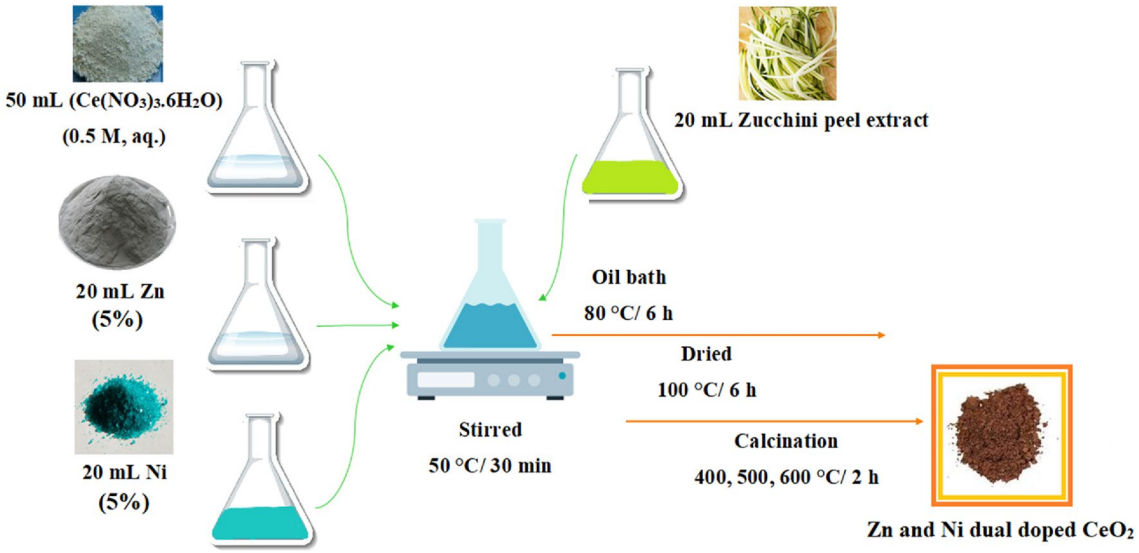

Fig. 1 Schematic of green synthesized Zn–Ni dual-doped CeO2-NPs

solutions were added dropwise into the A solution, to have the mixture solution (D) stirred for 30 min. Afterward, we appended 20.0 mL of *zucchini peel* extract to the D solution and transferred the mixture into the oil bath to be put under stirring at 80 °C for 6 h. The last step required the drying of obtained gel at 100 °C for 6 h, which was then calcinated at 400, 500, and 600 °C for 2 h. Figure 1 displays the green synthesizing schematic of Zn–Ni double-doped CeO_2-NPs.

Cytotoxicity

Cell culture

This experiment implicated the exertion of a liver cancer cell line (Huh-7), provided by the Pasteur Institute of Iran, for evaluating the cytotoxic impacts and enzymatic properties of synthesized Zn–Ni dual-doped CeO_2-NPs. The culturing of thawed cells was done within a DMEM medium enriched by 10% FBS, 100 µg/mL streptomycin, and 100 U/mL penicillin to go through incubation at 37 °C, 5% CO_2, and 95% air.

MTT assay

MTT assessment is a reliable colorimetric test for evaluating the cytotoxicity of Zn–Ni dual-doped CeO_2-NPs and determining the percentage of alive cells. The MTT experiment operates based on yellow tetrazolium salt breakage by succinate dehydrogenase enzyme and the production of purple crystals [22]. To start the procedure, the seeding of 100.0 µL of DMEM medium with 1×10^4 cells/well within a 96-well plate was completed to perform an incubation process for 24 h at 37 °C. Then, 100.0 µL of Zn–Ni dual-doped CeO_2-NPs with different concentrations (7.5–1000 µg/mL) was added into each well to be incubated for another 24 h. Afterward, we appended 20 µL MTT (5.0 mg/mL) to every well and conducted incubation again for 4 h at 37 °C. Once 50 µL DMSO was put into the wells, the purple formazan crystals were dissolved and, ultimately, the absorption of samples was read at 570 nm by an ELISA reader.

CAT and SOD antioxidant activity assay

The *CAT* and *SOD* activities were measured in different concentrations of CeO_2 (300, 700, and 1000 µg/mL) and Zn–Ni dual-doped CeO_2-NPs (100, 185, and 250 µg/mL).

CAT activity assay

The antioxidant activity of *CAT* was examined based on the method of Aebi (33) with a slight modification in accordance with the Teb Pazhouhan kit assay (Teb Pazhouhan Razi, Iran). Briefly, the *CAT* activity assay began by harvesting 1×10^6 cells/mL cells, which were then centrifuged at 1400×*g* for 5 min. Once 30 µL of methanol was mixed with 20 µL of the samples, 20 µL of hydrogen peroxide was added to the solution. Subsequent to 20 min of incubation at room temperature on a shaker, 30 µL of stopper reagent was appended to complete the reaction. Lastly, the absorbance was read at 540 nm.

SOD activity assay

The assessment of *SOD* activity implicated the reduction of tetrazolium salt in the presence of the superoxide anion that

resulted in the constitution of formazan dye. The hindered rate of exposed formazan to *SOD* could be measured through photometrical means. The *SOD* activity was accomplished in accordance with the manufacturing instruction of Teb Pazhouhan Razi, Iran. In summary, 10 µL of sample dilution buffer was added to 10 µL of the supernatant sample and 10 µL of double-distilled water, which was followed by the appending of 10 mL of *SOD* enzyme solution into the mixture. Afterward, we shook the prepared solution for 15 s and performed incubation at 37 °C for 20 min. The process ended by reading the absorbance at 440–460 nm.

Result and discussion

FTIR spectrum

Figure 2 represents the FTIR analysis of undoped CeO_2-NPs and Zn–Ni dual-doped CeO_2-NPs at the temperature of 300, 400, and 500 °C in the range 400–4000 cm^{-1}. Accordingly, the observed peaks at 3430 cm^{-1} and 1620 cm^{-1} were allocated to the stretching and bending vibrations of the O–H band of the H_2O molecule, respectively [23]. The other recorded peak at 1384 cm^{-1} was related to the remaining nitrates [24], while the peak at 1047 cm^{-1} was associated with the stretching vibration of O–Ce–O [25]. The exhibited peaks throughout the range of 400–1000 cm^{-1} were relevant to the stretching vibrations of metal–oxygen bonds [26–28].

UV–Vis/band gap

The UV–Vis spectra and band gap of Zn–Ni dual-doped CeO_2-NPs were investigated at 400, 500, and 600 °C in the range of 200–800 nm. As shown in Fig. 3a, Zn–Ni dual-doped CeO_2-NPs displayed suitable optical properties and seemed to contain maximum absorption bands at 347–351 nm, which were caused by the induced charge transfer from the O_2 (2p) orbital toward the Ce (4f) orbital [29]. The Zn–Ni dual-doped CeO_2-NPs exhibited a potent capacity to take photons as a result of their large surface and small size [30]. As shown in Fig. 3b, the band gap energy (Eg) of NPs was investigated by DRS analysis, (Table 1) and amounts of Eg were calculated from the Kubelka–Munk equation (Eq. 1). The results show that with the increase in temperature, the band gap energy decreases [31].

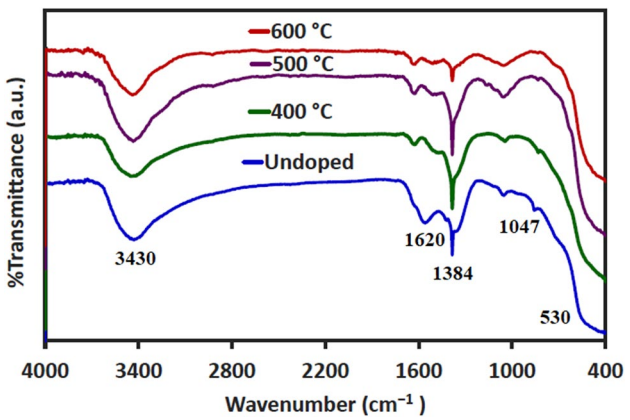

Fig. 2 FTIR spectra of undoped CeO2-NPs and Zn–Ni dual-doped CeO2-NPs

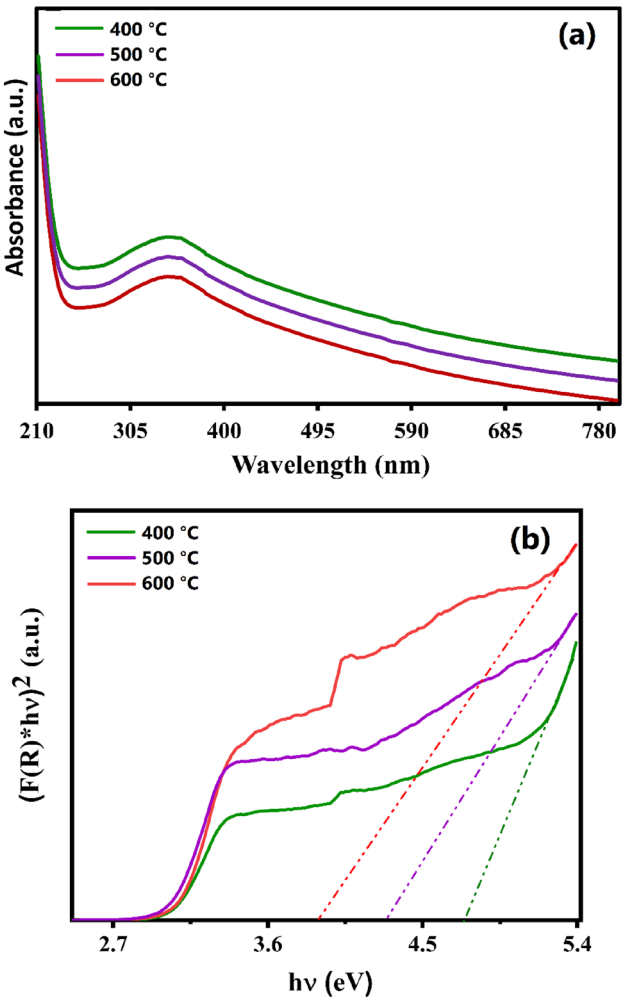

Fig. 3 UV–Vis spectra (**a**), energy of the band gap of Zn–Ni dual-doped CeO2-NPs

Table 1 Results of the band gap energy of Zn–Ni dual-doped CeO_2-NPs

Temp (°C)	λ_{max} (nm)	E_g (*e*V)
400	347.2	4.74
500	349.2	4.29
600	351.2	3.89

$$F(R) \times h\upsilon = A(h\upsilon - E_g)^n, \quad (1)$$

where A is the Constant number, fi υ is the photon energy, $n = 1/2$ direct gap and $n = 2$ indirect gap, and R is the reflection coefficient [32].

XRD pattern

Figure 4 demonstrates the XRD pattern of the crystalline structure of undoped CeO_2-NPs and Zn–Ni dual-doped CeO_2-NPs at 300, 400, and 500 °C in the 2Theta range of 10–80°. According to the results, the angles of 28.7°,33.3°,47.6°, 56.5°,59°,69.7°, and 76.9° were correlated with (111), (200), (220), (311), (222), and (400) planes, respectively. The XRD pattern exhibited the cubic fluorite state of the Zn–Ni dual-doped CeO_2-NPs crystal structure, which was consistent with JCPDS file 43-1002 [33]. The provided data by Scherrer's equation (Eq. 2) included the average crystallite size of NPs, which is presented in Table 2.

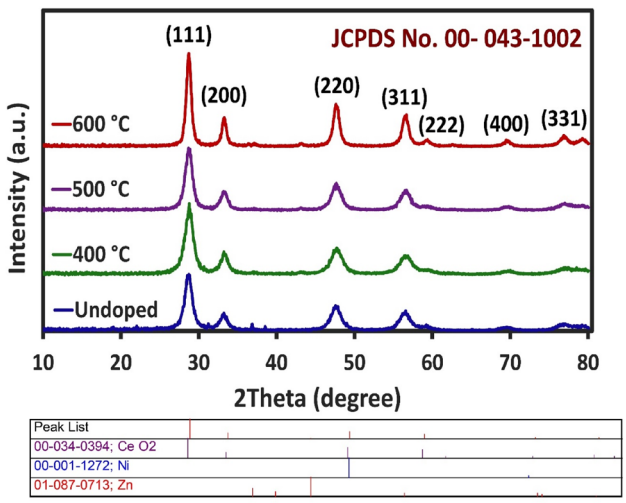

Fig. 4 XRD spectra of undoped CeO2-NPs and Zn–Ni dual-doped CeO2-NPs

Table 2 Relevance between the temperature and particle size

Temp (°C)	Diameter (nm)
Undoped CeO_2-NPs	
500	12.82
Zn–Ni–CeO_2-NPs	
400	9.25
500	11.87
600	21.09

$$D(\text{nm}) = \frac{\kappa\lambda}{\beta\cos\theta}, \quad (2)$$

in which D refers to the average particle size (nm), K displays the chosen constant of 0.9, $\lambda = 0.154$ nm, β stands for full width at half maximum, and θ presents the diffraction angle [34].

FESEM/PSA/EDX

FESEM/PSA/EDX analyses were included to investigate the size, distribution, and morphology of the synthesized Zn–Ni dual-doped CeO_2-NPs at temperatures of 400, 500, and 600 °C. According to the FESEM images [Fig. 5a (400 °C), Fig. 5b (500 °C), and Fig. 5c (600 °C)], Zn–Ni dual-doped CeO_2-NPs were uniform and almost spherically shaped in the range of nanoscale. In coordination with the PSA curves [Fig. 5d (400 °C), Fig. 5e (500 °C), and Fig. 5f (600 °C)], the size of NPs was increased as a result of heightening the calcination temperature, which was consistent with the XRD results. X-ray spectroscopy (EDX) is an analytical procedure for studying the chemical or structural properties of synthesized NPs. Based on the outcomes of this analysis [Fig. 5g (400 °C), Fig. 5h (500 °C), and Fig. 5i (600 °C)], Zn–Ni dual-doped CeO_2-NPs only possessed cerium, oxygen, zinc, and nickel, which signifies the complete purity of the synthesized NPs structure [35, 36].

MTT assay

The toxicity of undoped CeO_2-NPs and Zn–Ni dual-doped CeO_2-NPs with different concentrations (7.5–1000 µg/mL) on Huh-7 cells after 24 h is presented in Fig. 6a, b. IC_{50} is referred to as the concentration of undoped CeO_2-NPs and Zn–Ni dual-doped CeO_2-NPs that result in 50% of cell survival, which was around 700 and 185.4 µg/mL, respectively. Hence, the conduction of further studies and investigations on these NPs can hopefully lead to their application in the treatment of cancer [37, 38].

SOD and CAT activity assay for CeO_2 and Zn–Ni *dual-doped CeO_2-NPs*

We analyzed the antioxidant activity (*CAT* and *SOD*) of undoped CeO_2-NPs and Zn–Ni dual-doped CeO_2-NPs based on their cytotoxicity data. Considering the (IC_{50}) (Fig. 7 and Fig. 8), we selected the optimized concentrations of 700 and 185 µg/mL for undoped CeO_2-NPs and Zn–Ni dual-doped CeO_2-NPs, respectively. The activity of *SOD* in accordance with the one-way ANOVA test for both undoped CeO_2-NPs ($F(3, 8) = 20.86$, $P = 0.0004$) and Zn–Ni dual-doped CeO_2-NPs ($F(3, 8) = 31.98$, $P < 0.0001$) were significant.

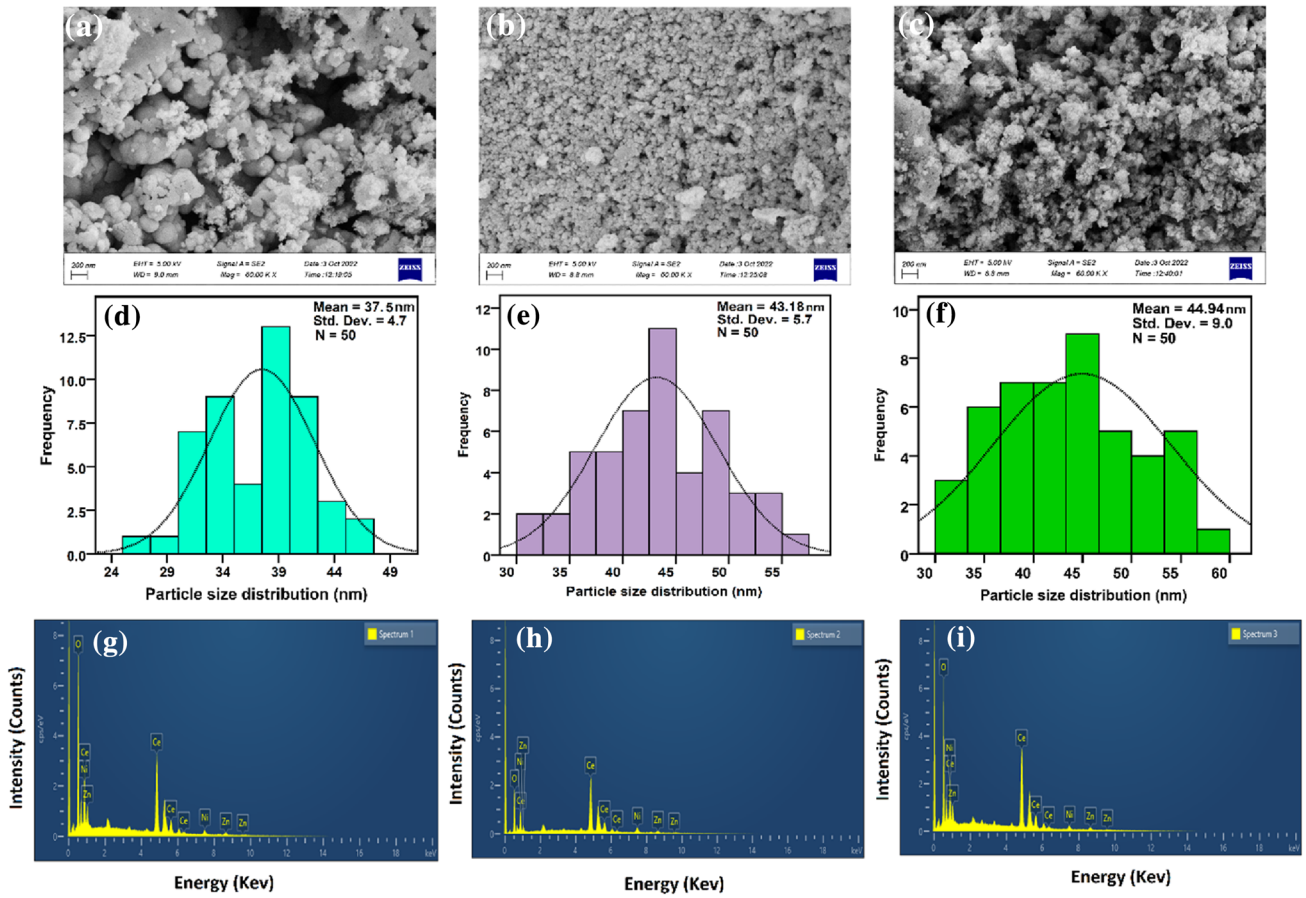

Fig. 5 The FESEM image (**a**–**c**), EDX analysis (**d**–**f**), and particle size (**g**—**i**) of Zn–Ni dual-doped CeO2-NPs

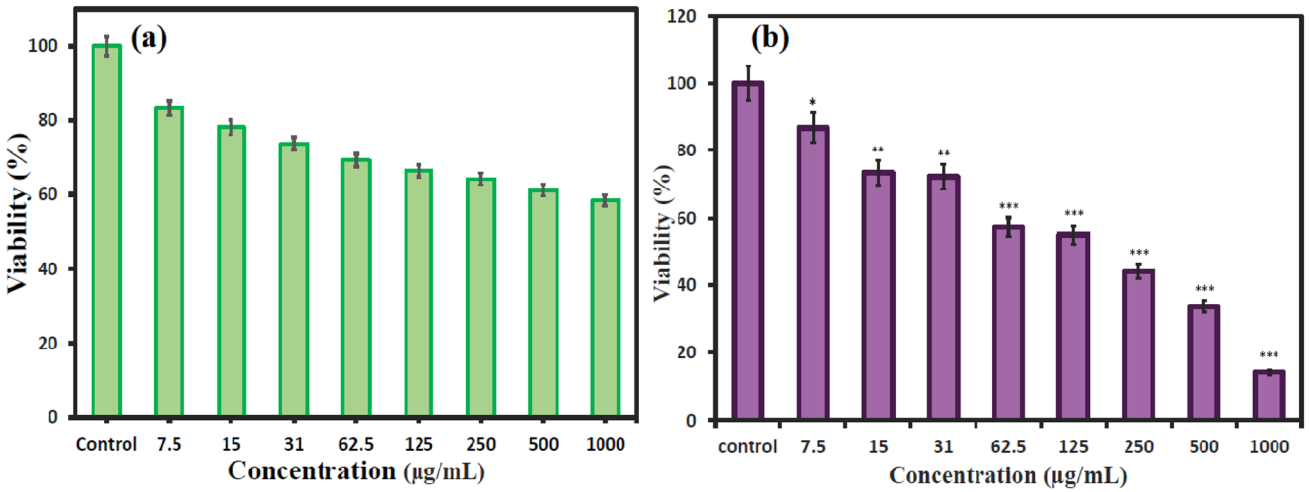

Fig. 6 In vitro effect of undoped CeO2-NPs and Zn–Ni dual-doped CeO2-NPs on Huh-7 cell through the MTT assay

According to Dunnett's multiple comparison tests, the concentrations of 700 (Mean Diff.: 0.7800, 95.00% CI of diff.: 0.03904–1.521, $P = 0.0399$) and 1000 µg/mL (Mean Diff.: 1.980, 95.00% CI of diff.: 1.239–2.721, $P = 0.0002$) for the cases of undoped CeO_2-NPs were significantly different in contrast to the control, while the volume of 300 µg/mL was

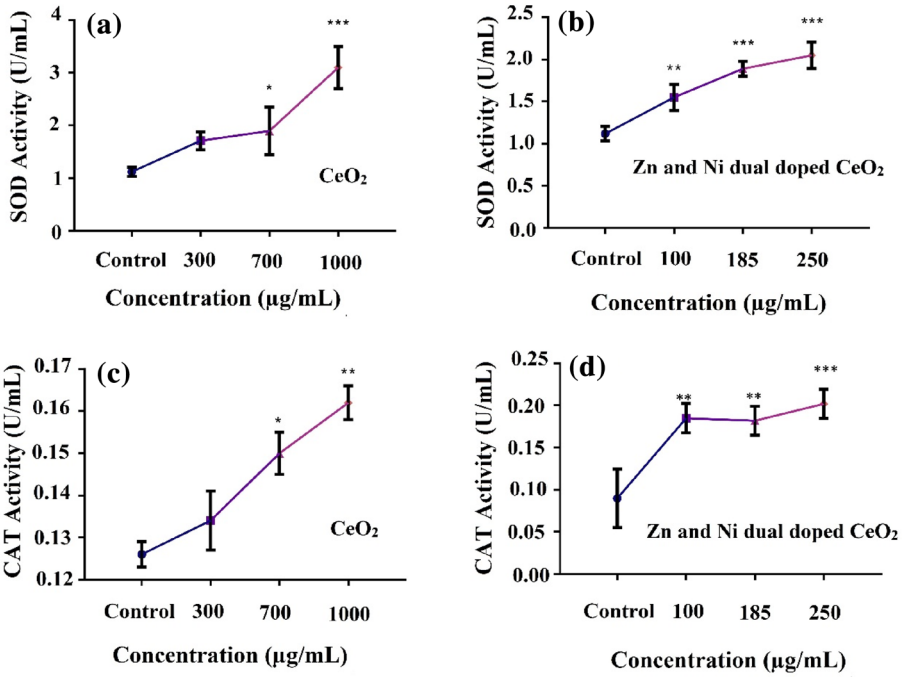

Fig. 7 The antioxidant activities of undoped CeO2-NPs. SOD activity of CeO2-NPs (**A**) and Zn–Ni duel-doped CeO2-NPs (**B**), CAT activity of CeO2-NPs (**C**) and Zn–Ni duel-doped CeO2-NPs (**D**). Data are shown as mean ± SEM. Statistical significances were provided in **P* value < 0.05 and ***P* value < 0.01, ****P* value < 0.001

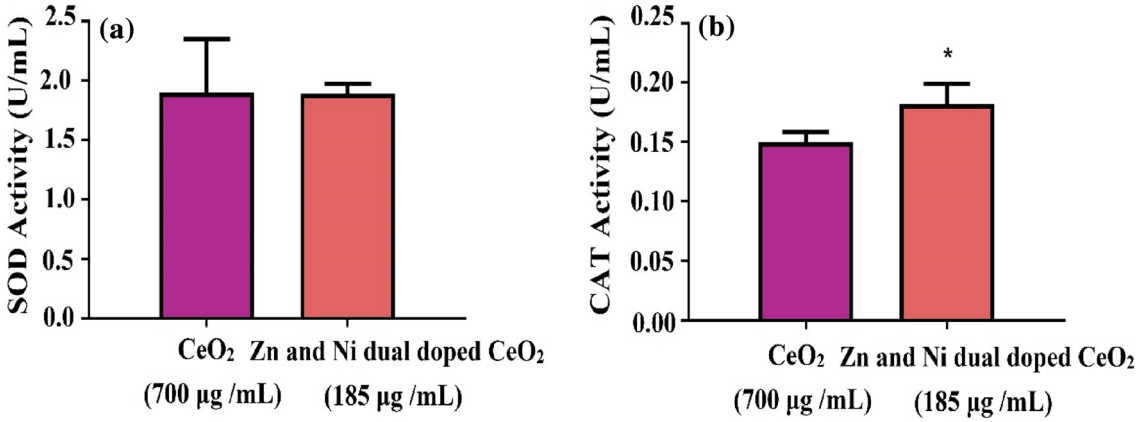

Fig. 8 Comparison of SOD (**A**) and CAT (**B**) activity between undoped CeO2-NPs and Ni-Zn dual-doped CeO2-NPs. Data are shown as mean ± SEM. Statistical significances were presented in **P* value < 0.05 and ***P* value < 0.01, ****P* value < 0.001

incapable of statistically displaying significant *SOD* activity (Fig. 1A). Furthermore, the trend analysis demonstrated the existing relation between the activity of *SOD* and increasing the applied concentration (R^2 0.9071, $P < 0.0001$). Moreover, every tested concentration of Zn–Ni dual-doped CeO_2-NPs was able to exhibit *SOD* activity. The data of linear trend (R^2 0.9634) was also indicative of the markedly dose-dependent *SOD* activity of Zn–Ni dual-doped CeO_2-NPs ($P < 0.0001$) (Fig. 1B). As an evident observation in *SOD* activity, similar antioxidant activities were displayed by Zn–Ni dual-doped CeO_2-NPs when compared to undoped CeO_2-NPs in lower concentrations (Fig. 2A). Significant outcomes were achieved by the one-way ANOVA test of both undoped CeO_2-NPs (F (3, 8) = 10.51, $P = 0.0038$) and Z–Ni dual-doped CeO_2-NPs (F (3, 8) = 14.64, $P = 0.0013$) in regards to *CAT* activity. Parallel to the *SOD* results, the means comparison tests of undoped CeO_2-NPs reported significant differences for the concentrations of 700 (Mean Diff.: 0.024, 95.00% CI of diff 0.003739 to 0.04426, $P = 0.023$) and 1000 µg/mL (Mean Diff.: 0.036, 95.00% CI of diff.: 0.01574 to 0.05626, $P = 0.0024$) in comparison to the control, while the lower concentrations lacked any notable *CAT* activity (Fig. 1C). As another similar outcome to the *SOD*, the trend linear analysis confirmed the dose dependability of *CAT* activity with increasing applied concentration (R^2 0.9856, $P = 0.0005$). However, the activity of the *CAT* enzyme in the

Zn–Ni dual-doped CeO_2-NPs concentrations of 100, 185, and 250 µg/mL was intensified. The regression analysis also confirmed the relationship (R^2 0.8459) of *CAT* activity with Zn–Ni dual-doped CeO_2-NPs ($P = 0.0005$) (Fig. 1D). A comparison between the *CAT* activity of undoped CeO_2-NPs and Zn–Ni dual-doped CeO_2-NPs indicated the significantly higher *CAT* activity of Zn–Ni dual-doped CeO_2-NPs than that of undoped CeO_2-NPs (Fig. 2B). In line with previous studies, our results also indicated the ability of undoped CeO_2-NPs and Zn–Ni dual-doped CeO_2-NPs to enhance the *CAT* and *SOD* activities. We also reported the higher efficiency of *CAT* activity in Zn–Ni dual-doped CeO_2-NPs when compared to undoped CeO_2, whereas the activity of *SOD* lacked the inducement of any changes in similar safety concentrations (undoped CeO_2-NPs: 700, Zn–Ni dual-doped CeO_2-NPs: 185 µg/mL).

A study by *Baldim, V.* et al. in 2018 on CeO_2-NPs reported the extreme reliance of CeO_2-NPs antioxidant activity on particle size and physicochemical features [39], as well as its dose-dependency that is correlated with extending the applied volume of CeO_2-NPs [40]. In conformity with previous research, our data also exhibited the strong dose-dependency of undoped CeO_2-NPs and Zn- Ni dual-doped CeO_2-NPs in regard to their antioxidant activities. Our in vitro observations were indicative of an increase in *CAT* and *SOD* activities subsequent to extending the concentration of undoped CeO_2-NPs and Zn–Ni dual-doped CeO_2-NPs, which probably confirms the mimic functionality of *CAT* and *SOD*.

Conclusions

The successful synthesis of undoped CeO_2-NPs and Ni-Zn dual-doped CeO_2-NPs was achieved through an eco-friendly method with the help of *zucchini peel* extract as a natural reduction agent. Among the various exerted methods for NPs synthesis, we employed a green synthesizing approach to exploit its benefits, which include cheapness, large-scale commercial manufacture, and possible pharmaceutical implementations when compared to other methods. The physicochemical properties of synthesized NPs were studied by the data of FTIR, UV–Vis, XRD, and FESEM techniques, which confirmed the spherical shape and purity of undoped CeO_2-NPs and Ni-Zn dual-doped CeO_2-NPs at the nanoscale. We also assessed the cytotoxic impacts of CeO_2-NPs and Ni–Zn dual-doped CeO_2-NPs on the Huh-7 cell line through the outcomes of the MTT assay. The capability of self-regenerating its surface is a notable feature of CeO_2-NPs that has outshined the other antioxidants. In other words, the application of one small dosage would be sufficient for a long duration. Our results proved the great antioxidant potential (*SOD* and *CAT* activity) of synthesized undoped CeO_2-NPs and Ni–Zn dual-doped CeO_2-NPs and also affirmed that an increase in the applied concentration of NPs would lead to intensifying the rate of antioxidant activity. Moreover, the implication of Zn and Ni metals resulted in improving the *SOD* and *CAT* activities.

Acknowledgements This project was financially supported by the Mashhad University of Medical Sciences and the Islamic Azad University of Neyshabur. This study is the result of a research project and thesis presented by Mrs. Pegah Mahmoodi.

Author contributions PM: investigation, methodology, software, writing—original draft, formal analysis. AM: investigation, software, writing—review and editing. MD: supervision, project administration, validation, methodology, writing-review and editing. JM: data curation, writing—review and editing. RZ: data curation, writing—review and editing.

Funding Not applicable.

Data availability Not applicable.

Declarations

Conflict of interest The authors declare no conflicts of interest regarding this article.

Ethical approval For this type of study, ethical approval is not applicable.

Consent to participate Not applicable.

References

1. Teeguarden JG, Hinderliter PM, Orr G, Thrall BD, Pounds JG (2007) Particokinetics in vitro: dosimetry considerations for in vitro nanoparticle toxicity assessments. Toxicol Sci 95:300–312
2. Esch F, Fabris S, Zhou L, Montini T, Africh C, Fornasiero P, Comelli G, Rosei R (2005) Electron localization determines defect formation on ceria substrates. Science 309:752–755
3. Walkey C, Das S, Seal S, Erlichman J, Heckman K, Ghibelli L, Traversa E, McGinnis JF, Self WT (2015) Catalytic properties and biomedical applications of cerium oxide nanoparticles. Environ Sci Nano 2:33–53
4. Heckman KL, DeCoteau W, Estevez A, Reed KJ, Costanzo W, Sanford D, Leiter JC, Clauss J, Knapp K, Gomez C (2013) Custom cerium oxide nanoparticles protect against a free radical mediated autoimmune degenerative disease in the brain. ACS Nano 7:10582–10596
5. Kargozar S, Baino F, Hoseini SJ, Hamzehlou S, Darroudi M, Verdi J, Hasanzadeh L, Kim H-W, Mozafari M (2018) Biomedical applications of nanoceria: new roles for an old player. Nanomedicine 13:3051–3069
6. Paul BD, Snyder SH (2019) Impaired redox signaling in Huntington's disease: therapeutic implications. Front Mol Neurosci 12:68
7. Dolgacheva LP, Berezhnov AV, Fedotova EI, Zinchenko VP, Abramov AY (2019) Role of DJ-1 in the mechanism of pathogenesis of Parkinson's disease. J Bioenerg Biomembr 51:175–188
8. Halliwell B, Gutteridge JM (2015) Free radicals in biology and medicine. Oxford University Press, USA
9. Thomas DT, DelCimmuto NR, Flack KD, Stec DE, Hinds TD (2022) Reactive oxygen species (ROS) and antioxidants as

immunomodulators in exercise: implications for heme oxygenase and bilirubin. Antioxidants 11:179
10. Celardo I, Pedersen JZ, Traversa E, Ghibelli L (2011) Pharmacological potential of cerium oxide nanoparticles. Nanoscale 3:1411–1420
11. Korsvik C, Patil S, Seal S, Self WT (2007) Superoxide dismutase mimetic properties exhibited by vacancy engineered ceria nanoparticles. Chem Commun 10:1056–1058
12. Heckert EG, Karakoti AS, Seal S, Self WT (2008) The role of cerium redox state in the SOD mimetic activity of nanoceria. Biomaterials 29:2705–2709
13. Shi X, Yang J, Wen X, Tian F, Li C (2021) Oxygen vacancy enhanced biomimetic superoxide dismutase activity of CeO2-Gd nanozymes. J Rare Earths 39:1108–1116
14. Pirmohamed T, Dowding JM, Singh S, Wasserman B, Heckert E, Karakoti AS, King JES, Seal S, Self WT (2010) Nanoceria exhibit redox state-dependent catalase mimetic activity. Chem Commun 46:2736–2738
15. Barrios AC, Rico CM, Trujillo-Reyes J, Medina-Velo IA, Peralta-Videa JR, Gardea-Torresdey JL (2016) Effects of uncoated and citric acid coated cerium oxide nanoparticles, bulk cerium oxide, cerium acetate, and citric acid on tomato plants. Sci Total Environ 563:956–964
16. Singh R, Singh S (2015) Role of phosphate on stability and catalase mimetic activity of cerium oxide nanoparticles. Coll surf B, Biointer 132:78–84
17. Gil D, Rodriguez J, Ward B, Vertegel A, Ivanov V, Reukov V (2017) Antioxidant activity of SOD and catalase conjugated with nanocrystalline ceria. Bioengineering (Basel, Switzerland) 4:8
18. Feng N, Liu Y, Dai X, Wang Y, Guo Q, Li Q (2022) Advanced applications of cerium oxide-based nanozymes in cancer. RSC Adv 12:1486–1493
19. Datta A, Mishra S, Manna K, Saha KD, Mukherjee S, Roy S (2020) Pro-oxidant therapeutic activities of cerium oxide nanoparticles in colorectal carcinoma cells. ACS Omega 5:9714–9723
20. Sisubalan N, Ramkumar VS, Pugazhendhi A, Karthikeyan C, Indira K, Gopinath K, Hameed ASH, Basha MHG (2018) ROS-mediated cytotoxic activity of ZnO and CeO_2 nanoparticles synthesized using the Rubia cordifolia L. leaf extract on MG-63 human osteosarcoma cell lines. Environ Sci Pollut Res 25:10482–10492
21. Palumbo JM, Hubble J, Apple S, Takei K, Tsuda K, Liu S, Zhang J, Agnese W (2019) Post-hoc analyses of the edaravone clinical trials study 16 and study 19: a step toward more efficient clinical trial designs in amyotrophic lateral sclerosis. Amyotroph Lateral Scler Frontotemporal Degener 20:421–431
22. Ananthalakshmi R, Rathinam SXR, Sadiq AM (2021) Apoptotic signalling of Huh7 cancer cells by biofabricated zinc oxide nanoparticles. J Inorg Organomet Polym Mater 31:1764–1773
23. Padmapriya G, Amudhavalli M (2020) Synthesis and characterization studies of spinel $ZnAl_2O_4$ nanoparticles prepared by Aloe vera plant extracted combustion method 2:2089–2091
24. Subbaiyan R, Ganesan A, Ramasubramanian B (2022) Self-potent anti-microbial and anti-fouling action of silver nanoparticles derived from lichen-associated bacteria. Appl Nanosci 12:2397–2408
25. Xu N, Ma J, Liu Q, Luo Y, Pu Y (2022) Preparation of CeO_2 abrasives by reducing atmosphere-assisted molten salt method for enhancing their chemical mechanical polishing performance on SiO_2 substrates. J Rare Earths. https://doi.org/10.1016/j.jre.2022.10.011
26. Karthik K, Shashank M, Revathi V, Tatarchuk T (2018) Facile microwave-assisted green synthesis of NiO nanoparticles from Andrographis paniculata leaf extract and evaluation of their photocatalytic and anticancer activities. Molecular crystals and liquid crystals 673:70–80
27. Sharma HR, Batoo KM, Neffati R, Dhiman P, Bhardwaj S, Sharma P, Hussain S, Sharma I, Goel R, Kumar G (2022) Investigation of structural, electrical and magnetic properties of $MnAlxFe_2$-xO_4 ferrite nanoparticles processed by solution combustion route. Physica B 646:414368
28. Sabouri Z, Sabouri M, Amiri MS, Khatami M, Darroudi M (2022) Plant-based synthesis of cerium oxide nanoparticles using Rheum turkestanicum extract and evaluation of their cytotoxicity and photocatalytic properties. Mater Technol 37:555–568
29. Kargar H, Ghazavi H, Darroudi M (2015) Size-controlled and bio-directed synthesis of ceria nanopowders and their in vitro cytotoxicity effects. Ceram Int 41:4123–4128
30. Kaewmuang P, Thongtem T, Thongtem S, Kittiwachana S, Kaowphong S (2018) Influence of calcination temperature on particle size and photocatalytic activity of nanosized NiO powder. Russ J Phys Chem A 92:1777–1781
31. Zak AK, Abd Aziz NS, Hashim AM, Kordi F (2016) XPS and UV–vis studies of Ga-doped zinc oxide nanoparticles synthesized by gelatin-based sol-gel approach. Ceram Int 42:13605–13611
32. Elahi B, Mirzaee M, Darroudi M, Oskuee RK, Sadri K, Gholami L (2020) Role of oxygen vacancies on photo-catalytic activities of green synthesized ceria nanoparticles in Cydonia oblonga miller seeds extract and evaluation of its cytotoxicity effects. J Alloy Compd 816:152553
33. Lin S, Zhang T, Zhang J, Pan X (2022) Preparation of Mg and Ce nanomaterials and their degradation of dye wastewater. J Mater Sci: Mater Electron 33:15156–15165
34. Miri A, Darroudi M, Sarani M (2020) Biosynthesis of cerium oxide nanoparticles and its cytotoxicity survey against colon cancer cell line. Appl Organomet Chem 34:e5308
35. Miri A, Sarani M, Khatami M (2020) Nickel-doped cerium oxide nanoparticles: biosynthesis, cytotoxicity, and UV protection studies. RSC Adv 10:3967–3977
36. Parvathy S, Venkatraman B (2017) Synthesis and characterization of various metal ions doped CeO_2 nanoparticles derived from the azadirachta indica leaf extracts. Chem Sci Trans 6:513–522
37. Darroudi M, Nazari SE, Karimzadeh M, Asgharzadeh F, Asghari SZ, Khalili-Tanha N, Rezayi M, Khazaei M (2023) Fabrication of magnetic nanocomposite as responsive drug delivery vehicle for cervical cancer therapy. Appl Organomet Chem 37:e7068
38. Darroudi M, Nazari SE, Asgharzadeh F, Khalili-Tanha N, Khalili-Tanha G, Dehghani T, Karimzadeh M, Maftooh M, Fern GA, Avan A (2022) Fabrication and application of cisplatin-loaded mesoporous magnetic nanocomposite: a novel approach to smart cervical cancer chemotherapy. Cancer Nanotechnol 13:36
39. Baldim V, Bedioui F, Mignet N, Margaill I, Berret J-F (2018) The enzyme-like catalytic activity of cerium oxide nanoparticles and its dependency on Ce^{3+} surface area concentration. Nanoscale 10:6971–6980
40. Es-haghi A, Nezhad SA (2019) The anti-oxidant and anti-inflammatory properties of cerium oxide nanoparticles synthesized using *Origanum majorana* L. leaf extract. Int Basic Sci Med 4:108–112